OPEN ACCESS
Global Journal of Research in Engineering & Computer Sciences
Volume 01| Issue 02 | Nov - Dec | 2021
Journal homepage: https://gjrpublication.com/journals/

Original Research Article

MGS decontamination of N95-like respirators: dielectric considerations

*Victor J Law[1] & Denis P Dowling[1]

[1]School of Mechanical and Materials Engineering, University College Dublin, Belfield, Dublin 4, Ireland

Submission Date: 22 Nov. 2021 | **Published Date:** 20 Dec. 2021

***Corresponding author:** Victor J Law

Abstract

Dielectric volume heating of water inside a microwave oven, can generate steam which in-turn can be used for the decontamination of surfaces against bacteria and viruses. This Microwave generated steam (MGS) has a number of potential applications, such as the decontamination of personal protective equipment. This paper focuses on the use of MGS for the decontamination of N95-like respirators, which are widely used to protect the wearer from airborne biological particles such as viruses and bacteria. This work examines the dielectric properties (real and imaginary parts of the complex permittivity, loss tangent and penetration depth) of the constituent parts of the batch MGS decontamination of N95-like respirators. The constituent parts being: distilled-water, tap-water, N95-like respirator, polypropylene material and, when present, the metal (aluminum) nose clip at a microwave oven cavity-magnetron operational frequency (f_o ~2.24 GHz, l_o ~12.2 cm).

This work proposes that N59-like respirator metal nose clip can be modeled as a quasi-transverse electromagnetic (TEM) microstrip, where at environmental temperatures (20 to 25^{o}C) the effective dielectric constant is defined by the surrounding polypropylene - air media. As the temperature increases to decontamination temperatures (70 to 100^{o}C), air is replaced with water vapor then stream causing the effective dielectric constant to increase and the phase velocity to decrease. Under these dynamic conditions, the imposed microwave wavelength is reduced causing the open- and short-circuit nodes to bunch and move along the aluminum conductor causing high voltage stress regions at the open-circuits nodes to momentarily align with sharp edges and protrusions resulting (with sufficient energy) to produce sparks and arcs. A literature search also reveals how the complex-load water volume, geometry non-rotation and rotation orientation within the horizontal-plan alter heating uniformity and the possibility of frequency pulling of the cavity-magnetron. This article demonstrates the links between complex-load dielectric parameters, cavity-magnetron stability, thermodynamics analysis the MGS decontamination of N95-like respirator.

Keywords: H1N1, SARS-CoV-2, N95 respirator, microwave oven, decontamination, dielectric, metal.

Introduction

In 2006-7 there was an acknowledgement (within medical journals) that US Strategic National Stockpile of N95 respirators would be in short supply when and if an influenza pandemic occurred[1,2]. In the UK short-fall in PPE was acknowledged by Public Health England[3]. Since 2009 world has undergone two influenza pandemics (caused by H1N1 and SARS-CoV-2), killing many of thousands of resulting in a dramatic shift in public perception of the role of governments, economic markets, and public healthcare systems. What started as a public health crisis into an due to the amount of single-use personal protective equipment, or PPE (e.g., N95 respirators and surgical respirators), used and then discarded, in the treatment of HINI and Covid-19 patients[4,5]. It is now considered that the world's post covid-19 economic recovery uses green and sustainable policies[6]. Driven by acute shortages of respirators in the 2009 pandemic, experimental batch MGS decontamination of respirators studies and reuse[7-12].

In 2020, Yap et al reported a dry-heat predictive decontamination model (excluding relative humidity and fomites) indicating that inactivation of all types of corona viruses, including SARS-CoV-2 may be achieved below the melting point (mp) range of functionalized polypropylene (f-PP) polymer that is commonly used in the manufacture of N95-like respirators[13]. [*N.B. pure isotactisc polypropylene (i-PP) begins to deform above 100°C and has an mp range of 160 to 171°C and*]. In the same year, Abraham et al[14] and Chin et al[15] presented data on the of SARS-CoV-2 on different fomites and environmental conditions. In addition, Viscusi et al[16] reported that 160°C oven dry-heat melted N95-like respirators. In Fischer et al (2020)[17] evaluated four different decontamination methods for SAR-CoV-2 virus inoculated N95-type respirators, ultraviolet radiation (260 to 285 nm), dry-heat (70°C), vaporized hydrogen peroxide (VHP), and ethanol (70%). Their result revealed that UV and VHP could be performed three times on respirators, dry-heat 1-2 times, whereas ethanol reduced N95 respirator integrity and should not be used. Also in 2020, five microwave-generated steam (MGS) decontamination comparative review studies[18-23] of[6-9], plus a 3M Technical Bulletin[24] of[6-9] where published. These demonstrated the effectiveness of MGS as a decontamination of bacteria and viruses[7-12]. Three further systemic comparative reviews (Probst et al[25], Schumm et al[26], and Seresirikachorn et al[27]) of[7-10] were published in 2021. In the same year, Loon et al reported on the reuse of respirators[28]. The MGS review paper described the experimental conditions of the industrial and domestic microwave ovens used and the respirator decontamination outcomes, however they did not evaluate the microwave energy conditions used by the free-running packaged cavity-magnetron (frequency of *fo* = 2.45 ±0.05 GHz (λ_o ~12.2 cm))[29,30, and 31]. For brevity, the magnetron is henceforth called a cavity-magnetron. During this period, Zalauf et al (June 2020)[32] used ceramic mugs, glass containers, and commercial microwave steam bags as the water reservoir within a microwave oven to decontaminate MS2 phage inoculated respirators. Plus, Pascoe et al (July 2020)[33] who used an industrial grade microwave oven (NE-1853; Panasonic) along with a commercial steam sterilizer to inactivate *Staphylococcus aureus* (*S. aureus*) inoculated N95-type respirators. From this new body of work, there appears to be some degree of separation in the physical heat decontamination of respirator process efficacy. That is, oven moist-heat, and MGS provide an increasing degree of decontamination / sterilization efficacy (> 3-$\log_{10}$ reduction in MS2 phage and >4-$\log_{10}$ influenza H1N1 virus for a exposure of sixty to ninety 90 seconds), rather than an oven dry-heat at 70°C for 90 minutes that produces a 2-3 $\log_{10}$ reduction of *S. aureus* on inculcated respirators[33]. In addition Viscusi et al (2007)[16] has shown that oven dry-heat at 160°C for 20 minutes results in melting of respirators containing f-PP. Figure 1ac schematically depicts this relationship between slow oven dry-heat (1a), and oven moist-heat (1b) and rapid MGS dielectric volume heating (1c) systems, also see table 1.

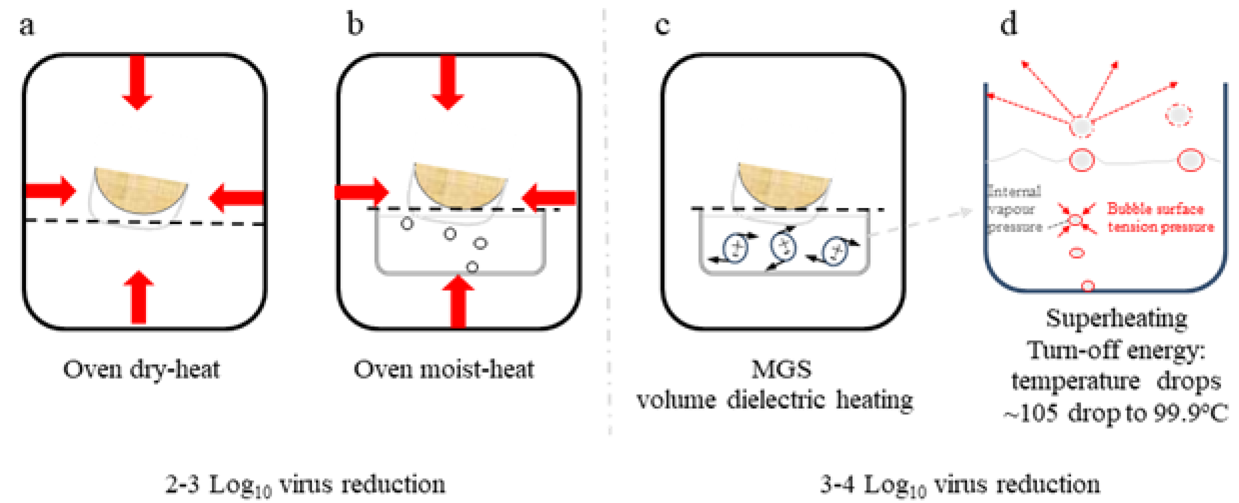

Fig-1: ad. Batch oven dry-heat a), oven moist-heat b), rapid MGS c), and microwave water superheating d).

The term 'rapid' as used by Gedye et al in 1988[34] and used again by Gedye et al in 1991[35] has differentiated the speed of dielectric volume heating with respect to the slow thermal heating of polar molecules such as water. In 1998, Tanaka et al[36] reported on moist towels inoculated with *S. aureus*, *Pseudomonas aeruginosa* and *Candida albicans* are sterilized using a domestic microwave oven (Corona Co., Ltd., Tokyo) set at rated microwave power of 2.45 GHz; 500 W for 1 to 2 minutes depending on the towel size. In 2006, Park et al used a domestic microwave oven to decontaminated kitchen sponges and scrubbing pads that were inculcated with *E. coili* wastewater[37]. Also around this time plastic-based infant feeding equipment designed for microwave oven steam sterilization became available for purchase[38]. This microwave treatment was wildly accepted as a cost efficient and simple to use home technology. By 2014, Wu and Yao[39] reported that a 1.7-minute direct microwave irradiation exposure at three different rated power levels (119, 384, 700W) achieved a 90% inactivation of MS2 virus. In their results, scanning election microscope imaging of microwave exposure virus, demonstrated its effect in rupturing surface.

Table-1: General overview of advantages and disadvantages of green chemistry decontamination; oven dry-heat and MGS [17,33, 40, and 41].

Decontamination process	Current advantages[33]	Current disadvantages [17, 33]	Process intensification improvements[40,41]
Oven dry-heat Typically 70 for 90 minutes	Used with N95 and N95s respirators Used with Type I and II masks Home ovens available for multiple respirators	Melts respirators at 160°C Slow compared to MGS Low decontamination efficacy May not eliminate odor	
MGS Typically at a rated 750 W magnetron power for 1 to 1.5 minutes	Rapid compared to dry-heat Broad spectrum of activity Essential oils can be added to impart fragrance and remove odor	Single batch process Incompatible with Type-I, II masks Induced arcing a partial separation in some types of N95 respirators Surgical respirators retain water after decontamination	Redesign sterilizer for multiple to hold respirators design respirator without metal noise clip, improve glue adhesion properties use material with lower water adhesion and retention properties

analysis of the application of MGS for the decontamination of respirators highlighted its green chemistry principles, in reducing the amount of harmful chemical products in the environment, as well as limiting the number of respirators required to be manufactured[40,41]. This thermodynamic analysis used the calorimetric method to calculate the total process energy budget, see linear equations (1) and (2).

$$P = mC\frac{\Delta T}{t} \quad (1)$$

Where P is the rated (or applied) cavity-magnetron power measured in units of Watts (J.s^{-1}, or W), m is the mass of the water (kg m^{-3}), C is the specific heat capacity of water (4.184 J g^{-1} K^{-1}), ΔT is the change in water temperature (final temperature minus the initial temperature), and t is the heating time measured in seconds.

$$Q = mC\Delta T \quad (2)$$

Where, Q is the specific heat (measured in Joules) to raise the amount water to 99.9°C. The additional process energy is calculated from the total process time minus the time taken to raise water to 99.9°C at the rated (applied) power of the cavity-magnetron(s). The knowledge gained from this linear thermodynamic analysis allows a greater understanding of the complex MGS decontamination of respirators and gives a direction for future research.

The thermodynamic process energy budget (in terms of energy input and output) parameters[7-10] reported a number batch MGS decontamination papers related to the 2009 influenza pandemic are presented in table 2. The MGS papers[32,33] that are a response to the 2019 influenza pandemic are given in table 3.

Table-2: Batch MGS decontamination papers response to the 2009 influenza pandemic. Energy input calculations (columns 2 and 3), energy output calculations (columns 6 to 8).

Author	Energy input calculations		Energy output calculations				
	Power (W)	Process budget (kJ)	Water (g)	99.9°C - room temperature (ΔT) [a]	heat energy Q (kJ) used to reach 99.9°C	Energy for steam conversion (kJ)	Liquid (g) into *steam (L)*
Bergman [7]	750	90	100	80	33.5	56.5	25 *41.7*
Heimbuch [8]	1250	150	100	76.5	32	118	52.2 *87.2*
Fisher [9]	750	65.5	60	78	19.6	45.9	20.3 *34*
Lore [10]	1250	150	50	78	16.3	133.7	59.2

							98.8

The grey shading of [7,9] data differentiates the average measured rather than a rated cavity-magnetron power.

Table-3: Batch MGS decontamination papers response to the 2019 influenza pandemic. Energy input calculations (columns 2 and 3), energy output calculations (columns 6 to 8).

Author	**Energy input calculations**		**Energy output calculations**				
	Power (W)	**Process budget (kJ)**	**Water (g)**	**99.9°C - room temperature (*ΔT*)**	**heat energy Q (kJ) used to reach 99.9°C**	**Energy for steam conversion (kJ)**	**Liquid (g) into *steam (L)***
Zulauf [32]	1100 1150	202.5 [a]	60	78	19.6	185.3 [i]	81.8 *136.6*
Pascoe [33]	2 x 900	162	200	80	66.9	95.1	42 *70.2*

[a] Mean process budget for the two cavity-magnetrons [32].

It is interesting to compare the performed of MGS generated within a domestic microwave oven that employs a 2.45 GHz cavity-magnetron, for the decontamination of surfaces with that of atmospheric plasma generated treatment systems. Examples of the a cross-field atmospheric pressure plasma jet to inactive SARS-CoV-2 on metal, plastic and leather surfaces was published in 2020 by Chen et al[42] and; in 2021 by Capelli et al[43] who used a dielectric barrier discharge generating a plasma treatment area of 551 cm^2 to inactive SARS-CoV-2 on plastic and metal surfaces. For these plasma systems, decontamination treatment of the outside and inside surfaces of N95-like respirator require the plasma systems to be mounted on a computer numeric controlled (CNC) table to facilitate full coverage of the N95 respirator, which has a typical face width 13.59 cm and length 11.7 cm[44]. No such CNC system is required in the case for MGS, thus indicating its ease of application of decontamination technology. In paper published by the current authors[41] scale-out by process intensification of the experimental MGS decontamination of N95-lik respirator process[7-10,32 and 33] was also proposed.

The aim of this article is consider the dielectric properties of liquid-phase water and water-gas phase change interacts with N95-like respirators within a microwave multimode-cavity. Using his knowledge a better understanding and improvement of batch MGS decontamination of N95-like respirators process may be obtained. The safety prevention of potential scalds and burns[45,46] of MGS process is important has been examined[40,41] and therefore will not be covered here. This article is constructed as follows. Section 2, examines the physical construction of N95-like particle and SN95-like (surgical) respirators. Section 3 examines of the dielectric properties of distilled water and tap-water, and polypropylene, and where present, respirator metal nose clip in the context of batch MGS decontamination of N95-like respirator processing. Comments on cavity-magnetron rated and available power and temperature measurement. Finally, section 5 provides a summary this article.

2. N95 particle respirators and surgical respirators

Today particle respirators are manufactured in two types of shape: preformed cup-shaped and flat-folded. The American (N95) European (FFP2) and China (KN95) particle respirators are considered medical devices for health professionals. They are designed to achieve a very close facial fit and very efficient filtration of airborne penetrating particles[47-50]. When new and fitted correctly respirators provide personal protection (filter ≥ 95% of 0.3 micron airborne particles (hence the term 95 in the America and Chinese standard). The surgical respirator (SN95) is a subclass of the N95-FFP2-KN95 respirator and designed as a loose-fitting device that creates a physical barrier between the mouth and nose of the wearer with the aim to prevent large droplet splashes and bodily fluid in the immediate environment.

A further subclass of the N95-like respirator is the N95 oxygen (O_2) respirator that is fitted with an oxygen manifold for supplying supplementary O_2[48]. Typically, N95-like respirators have an outer and inner semi-rigged barrier layer made of f-PP which provides mechanical support and filtration. Within these two layers a middle layer comprise f-PP meltblown nonwoven microfibers with diameters of 2-10 microns with a unimodal positive skewness distribution profile (fig 2d) all of which are roughly aligned parallel to the layer[49-51]. The few thick diameter microfibers provide scaffolding support for the small diameter microfiber when a 3-dimensional mesh with both loft and void space that allow a porosity of 90% and high air permeability. The mesh barrier micron filtration efficiency is improved by adding a quasi-permanent electrical charge (electrets) to microfibers corona discharge whilst keeping the same high air permeability. Figure 2e provides schematic of a meltblown microfiber layer that progressively captures harmful particles in the direction of airflow (outside to inside of the respirator).

Some N95-like particle respirator designs (3M-2810) incorporate a metal nose clip on the upwards and outer side of the respirator body. Figure 2a depicts one such respirator. The role of the clip is to enhance the respirator-to-face seal. Generally, the metal clip is made of aluminum with a physical length (l) ~ 10, width (w) ~ 0.5 and depth (d) ~ 0.1 cm and glued to the respirator body. The manufacturing process of these clips generally involves a stamping-out process that can leave small but measureable sharp edges.

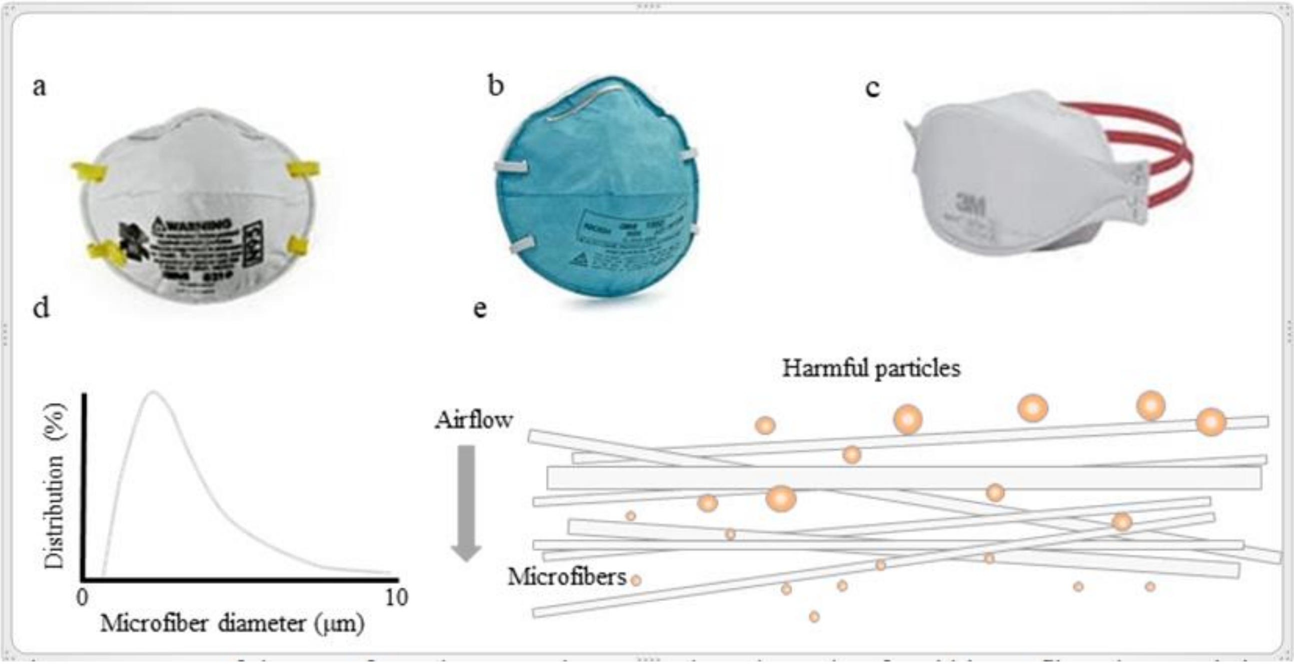

Fig-2: ae. Images of three preformed 3M respirators, and a schematic of meltblown fiber characteristics. 3M-2810 N95 particle respirator a), 3M-1860 N95 surgical respirator b), 3M-1870 surgical respirator c), schematic of meltblown microfiber layer along with the direction of harmful particle capture d) and typically microfiber diameter distribution e).

3. Dielectric considerations for batch MGS decontamination of N95-like respirators

The industrial scientific medical (ISM) band radio spectrum for RF welding, industrial heating, and microwave ovens without a license. The 0.915 ±0.025 GHz and 2.45 ±0.05 GHz bands are the most common bands for continuous inline industrial food processing and batch food processing within a domestic microwave oven[52,53].

In this frequency band, there are two main mechanisms of microwave heating of liquid-phase water. The first mechanism is dipole reorientation by the microwave electric field that cause in internal rotation casing frictional heat generation within the water molecule to volumetric heating of the water volume. The second major mechanism is ionic conduction is linked to the ability of ions to migrate under the influence of the electric field and generate heat. For these reason dielectric properties of the material in involved in batch MGS decontamination of N95-like respirations, rather than the permittivity properties, are considered in this work.

The following considerations include: distilled-water and tap-water (section 3.1), dielectric properties of f-PP (section 3.2), microwave interaction with preformed N95-like respirator metal nose clip (section 3.3), microwave superheating and steam bubble growth (section 3.4), the water reservoir heating within complex-load (section 3.5), steam-respirator interaction within complex-load (section 3.6). Comments on cavity-magnetron rated and available power (3.7). Finally section 3.8 examines corona virus interaction with microwave irradiation.

There are four fundamental properties that measure a polar solvent (water), nearly non-polar (polymers), and metals response to a microwave electric field at a given temperature**.** The first two are the permittivity or dielectric constant (ε_r'), and the dielectric loss factor (ε_r''). Where ε' is a measure of the materials ability to couple with microwave energy and ε'' is used as a measure of the materials ability to be heated by absorb microwave energy and turned into heat. Both of these properties can be expressed through the following complex notation: $\varepsilon, = \varepsilon_r' \text{-} j\, \varepsilon_r''$ that has a dimensionless number where ε_r' is the real-part ε_r'' is the imaginary-part, and j is the complex constant. The third property is the loss tangent, or loss angle, as expressed by $\tan\, \delta_e = \varepsilon_r'' / \varepsilon_r'$ is related to the substance susceptibility to be penetration by an electric field and dissipate electrical energy to heat. Lastly, the penetration depth (dp) is a measure of how deep microwaves can penetrate into the material that is being irradiated. It is defined as the depth where the dissipated power is reduced to e^{-1}

(approximately 37%) of the initial power entering the surface. Table 4 lists the value of these properties for the following materials (at 2.45 GHz for an initial environmental temperature of 20 to 25°C and decontaminant temperature of 100°C: air, distilled-water, tap-water, f-PP, and aluminum. References are given for the listed material properties, where the measured frequency and temperature is different, the values are highlighted. Given that the dielectric properties are independent of both frequency and temperature, a dynamic, or nonlinear, rather than a linear as in the case of thermodynamic analysis, obtained for the MGS decontamination process.

Table-4: Real and imaginary complex permittivity, *tan* δ_e and penetration depth at 2.45 GHz for an initial environmental temperature (20 to 25°C) and a decontamination temperature of 100°C.

Substance	$\varepsilon_r{'}$ 20 to 25°C	$\varepsilon_r{''}$ 20 to 25°C	$\tan\delta_e$ $\varepsilon_r{''}/\varepsilon_r{'}$	*dp*	$\varepsilon_r{'}$ at 100°C	$\varepsilon_r{''}$ at 100°C	$\tan\delta$ $\varepsilon_r{''}/\varepsilon_r{'}$	*dp*
Air [52]	1							
Distilled-water [53, 54, and 55]	~78	~12.5	~0.16	~1.3 cm	~ 55	~2.5	~ 0.045	~5.7 cm
Tap-water [54, 55]	~70	~ 10	~ 0.14	~1.6 cm	~ 55	~2.5	~ 0.045	~5.7 cm
i-PP [56 - 59]	~2.4	~ 0.0002	~1 x 10^{-5}	150 m	~2.2 [b]	~0.0002	~1 x 10^{-4}*	143 m
Aluminum [52,61]	~ 18.5	~0.3	0.01	1.7 μm	~17.2 [c]	~0.25 [c]	0.04 [c]	1.7 μm

[b] measured at 9.45 GHz [56], [c] measured at 70°C [60].

3.1 Distilled-water and tap-water

Abdelgwad and Said 2015[54] and Komarov and Tang (2004)[55] have published the dielectric properties of pure (distilled) and chlorinated (0.1 to 0.5 to mg l^{-1}) tap-water in the microwave region of 0.5 to 5GHz and 0.915 GHz, respectively. This work, uses their dielectric data as a reference source, see table 4.

3.2 Dielectric properties of polypropylene

The nearly nonpolar thermoplastic polypropylene resin (r-PP) has a simple hydrocarbon repeat chain structure $\left(-CH_2 - \underset{CH_3}{CH} -\right)n$ And is the most common starting polymer used in the manufacture of N95-like respirators[47-51]. The dipolar impurities (end groups, chain folds, and branch points) within the hydrocarbon chain are generally considered the origin of the dielectric loss[56-59].

Figure 3 shows the structure formula (without impurities) of the three basic PP homopolymer chains (atactic (amorphous), syndiotactic, and isotactic). In this figure, the substituents relate to the orientation of the side methyl groups. The generally accepted thermal deformation temperature of i-PP is in the region of 100°C and mp region between 161 and 171°C[58,59].

To obtain the ideal melt flow index required for the production of meltblown nonwoven microfibers, the crystalline i-PP polymer is mixed with other natural and synthetic polymers plus specific nanomaterials[60] to synthesis the final f-PP. As with the variation of mp of r-PP, the dielectric properties of the f-PP depend upon its tacticity and crystallinity. Unlike end groups and branching, repeat respirator donning and negative pressure user seal checks may induce polymer chain folding which may induce dielectric. In this work, the generally accepted value of $\varepsilon_r{'}$ and $\varepsilon_r{''}$ for i-PP are listed in table 4.

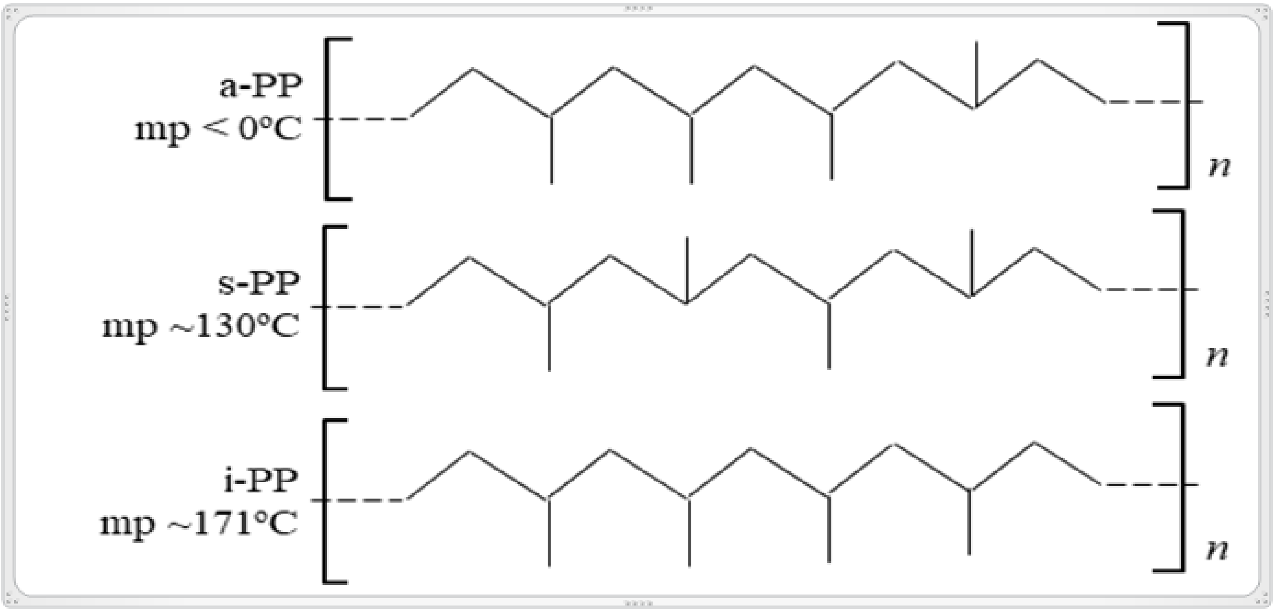

Fig-3:Skeletal structural of homopolymer polypropylene a-PP (atactic PP), s-PP (syndiotactic PP), and i-PP (isotactic PP). The methyl groups are implied and the impurities are not shown, and the name and the upper mp limit are given to the left of each polymer structure.

3.3 Microwave interaction with N95-like respirator metal nose clips

From an electromagnetic point-of-view the N95-like respirator metal noise clip construction, in air, acts like a microstrip operating in a quasi-transverse electromagnetic (TEM) mode and is effectively independent with the environmental and decontamination temperatures discussed here, see figure 4.

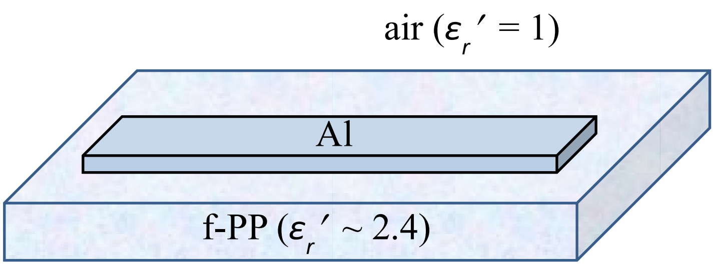

Fig-4: Schematic diagram of proposed aluminum nose clip microstrip surrounded with air and f-PP.

Given this knowledge, a simple two layered approach to defining the effective dielectric constant (ε_l) around the aluminum nose clip can be approximated as an average of the real-part of the complex dielectric constant of air and f-PP.

$\epsilon_l \sim \frac{\epsilon_r{}' + 1}{2}$ (3)

Therefore, ε_l is approximately 1.7 at an environmental temperature of 20 to 25°C, and at a decontamination temperature of 100°C ε_{reff} falls slightly ~ 1.6.

The phase velocity (v_p) of the microstrip is slower than the velocity of light (3 x 10^8 m s^{-1}) by the inverse of ε_l and approximates to equation 4.

$v_p \sim \frac{1}{\epsilon_l}$ (4)

Thus for the f-PP and air combination, the wavelength of an imposed standing wave structure on the microstrip will be 0.57 less than it would be in free space. For example, a 10 cm straight length (not bent) sample of the nose clip microstrip when irradiated at 2.45 GHz, one full wavelength (λ_m) will correspond to approximately 7 cm (equation 5) or nearly ¾ of the physical length of the microstrip to produce short- and open-circuit nodes every 2.5 cm.

$$\lambda_m \sim \frac{c\, v_p}{f_o} \quad (5)$$

As the MGs decontamination proceeds, the surrounding air is expected to be replaced by water vapor and ultimately steam that envelopes the respirator, to facilitate decontamination at these elevated temperatures, the aluminum nose clip microstrip e_{reff} increase and v_p decreases. If distilled-water or tap water is used, the aluminum nose clip microstrip has an approximate ε_{reff} value of 28.7 and an approximate v_p of 0.035 that generates 25 full wavelengths along length of the clip, with short- and open-circuit nodes every ¼ wavelength.

For batch MGS decontamination process to be efficient successful, the microwave irradiation needs to penetrate both the water reservoir whether it is an open water bath or sterilizer. A useful measure of how deep microwaves can penetrate into a material that is being irradiated is defined as the penetration depth (d_p) where the dissipated power is reduced to e^{-1} (approximately 37% of the initial value at the surface). The magnitude of the d_p determines whether the microwave will be reflected, transmitted, or absorbed by a material. Accordingly, a metal, such as aluminum, that has a d_p value of a few microns prohibits the penetration of microwaves and is classed as reflectors[52,61]. Functionalized PP, has $\tan \delta_e < 0.01$ or d_p of the order of a meter are class as transparent. High-loss materials with $\tan \delta_e > 0.1$ or d_p of the order of a cm such as water can absorb microwaves and convert energy in to heat. One formulation of d_p is given in equation 6.

$$d_p \sim \frac{\lambda_0 \sqrt{\epsilon'}}{2\pi\epsilon''} \quad (6)$$

Given that microwave irradiation of 2.45 GHz has a $\lambda_o = 12.2$ cm, 2 and π are constant, the ratio of square root of ε_r' divided by ε_r'' provides a measure of the microwave irradiation heating efficiency at a given temperature. The computed d_p valves for distilled-water and tap-water (see table 4) reveal that local microwave power absorption increase with temperature in the range of 20 to 100^{o}C: whereas for the low-loss f-PP, microwave power absorption does not insignificantly change in this temperature range.

In the microwave oven, aluminum is also expected to undergo two specific interactions with microwave irradiation that can generate local sparks and arcs.

Firstly, as the microstrip phase velocity decreases the open- and short-circuit nodes move along the aluminum conductor, momentary alignments of high voltage stress (V cm^{-1}) at the open circuit nodes align with sharp edges and protrusion on the aluminum surface result in local gas breakdown, corona discharge and plasmoids, and with sufficient energy transform into sparks and arcs.

Secondly, with the aluminum penetration depth of the order of a few microns most of the microwave irradiated energy is reflected. The small amount of microwave energy that penetrates the surface region interacts with free elections to induce surface eddy currents to flow. As the free electrons move they become attracted to surface sharp edges and irregularities resulting in again high voltage stress (V cm^{-1}) regions that cause the free electrons to be liberated leading to a local gas breakdown, corona discharge and plasmoids, and with sufficient energy transform into sparks and arcs.

Both of these interactions with sufficient temperature can ignite and burn the f-PP polymer, followed by melting of metal nose clip. If the microwave irradiation continues, the reflected microwave energy from the discharge reinforces the microwave standing pattern within the multimode-cavity to such a level that the reflected energy disrupts the operation of the cavity-magnetron causing the oven's internal circuits to stop working, or in the extreme case setting the oven on fire. Since the 1990s, near-filed probes projecting into multimode-cavity have been used to detect a local voltage stress levels that induces sparks and arcs within the cavity, and with monitoring and control circuitry the signal it is used to automatically shut-down the oven before an electrical fire is initiated[62].

3.4 Microwave Superheating and steam bubble growth

The phenomenon of polar solvent superheating is well known and commonly used in microwave assisted chemistry[34-38]. Unlike thermal hearting of liquid-phase water where heat is transferred from the outside to the inside, the microwave energy heats water molecules directly by the volume dielectric heating (figure 1c). At atmospheric pressure, and in the initial stage of volume heating, water is still in a single liquid-phase, and evaporation only occurs at the free-surface. Bubble growth is slow, as the bubble external pressure and membrane surface tension is greater than the bubble internal vapor pressure thus causing the embryonic bubbles to remain at their nucleation sites, whether on the vessel wall or on salt crystals and other mineral impurities within the. At 2.45 GHz, Lee et al (2020)[63] has numerically shown that in the initial (first) stage of volume dielectric heating of 200 ml of non-stirred distilled-water (a similar volume of water reported in many MGS decontamination of respirator papers) the liquid-phase undergoes considerable degree of local heating that generate convection forces to generate stratification within the liquid phase water. For 0.915 GHz the heating rate of liquid-phase water is greatly reduced[64].

After period of heating the liquid-phase approaches saturation temperature where bubble nucleation is promoted forcing the destruction of the stratification. At this point of superheating of water occurs when heat transfer in to the water volume is rapid and greater than the water evaporation rate. In the second stage of heating where saturation temperature has been reached, bubbles nucleation increase, grow in size, and become released allowing them float to the free-surface causing the removed of heat from the bulk of the water. As the air bubbles grow in number, a heterogeneous two-phase mixture is developed within the water bulk. The dissolved nature of the air bubbles alters the water dielectric constant and is defined as (ε_m) where the subscript m is the liquid-bubble mixture. One such rule of the many[65] for ε_m is given by Looyenga (1965)[66] and given here as the cubic formula for the volume fractions (equation 7) where the subscripts denote the liquid and gas vapor phase and α_g is the vapor fraction.

$$\varepsilon_m = \left[\left(\varepsilon_g^{1/3} - \varepsilon_l^{1/3}\right)\alpha_g + \varepsilon_l^{1/3}\right]^3 \quad (7)$$

As superheating can generate temperatures of 105°C, successful respirator decontamination becomes problematic due to the f-PP deformation begins above 100°C which at long exposure times will be detrimental to loft and voids within the f-PP meltblown material. There are a number of ways of achieving this goal, by replacing distilled-water with tap-water, introduce anti-bump granules, use an submerged array of metal wire aerial electrodes[29] or use a microwave transparent glass or plastic vessel that has scratches and sharp edges.

3.5 Water reservoir -respirator within complex-load

In this work, the term complex-load is used to describe the combined volume of the liquid-phase water, liquid-gas phase state, and N95-like respirator, where each component has differing dielectric properties that change with local temperature. The challenge here however is that the complex-load volume, geometry, non-rotation and horizontal-plane rotation orientation within a microwave oven multimode-cavity provides a series of design variables with respect to uniform dielectric volume heating. For example, Geedipalli et al (2007)[67] demonstrated that an irregular shaped potato (typically l ~ 3.6, w ~ 4.7, d ~ 2.1 cm with $\varepsilon_r{}'$ and $\varepsilon_r{}''$ of 57 and 17, respectively[68]) presents a rotational orientation challenge to uniform heating. Figure 5 shows the typical location of a complex-load within a domestic microwave oven. For example, the reported experimental batch MGS decontamination papers[7-10,32 and 33] used either a rectangular open water bath or a semi-round sterilizer, each of which typically contains 100 ml of water per cavity-magnetron. For the open water bath method, Zalauf et al[32] has shown that the open water bath free-surface needs to be approximately twice the presented area of the respirator for complete (all-over) respirator decontamination. This surface area criteria, equates to an open water bath with typical linear edges of l ~ 12, w ~ 8, d ~ 4.5 cm containing an initial 100 ml liquid-phase water to a depth of 1.05 cm within a typical domestic microwave oven employing a single cavity-magnetron side-illumination. For the industrial microwave oven, two cavity-magnetrons may be used[33] where the initial liquid-phase water depth equates to 2.1 cm.

The water volumes used in the batch MGS decontamination papers[7-10, 32 and 33] fall into the region where the heating outcome is domestic microwave oven specific. This was highlighted for the volume dielectric heating off a water-load by Houšová and Hoke and reference within. Their results revealed, for water-loads >200 ml the heating efficiency is oven specific, whereas above 250 ml the heating efficiency becomes independent of the water-load volume. In the extreme lower case where the microwave oven is operated with an empty (unloaded) multimode-cavity, the cavity-magnetron is likely to be damaged.

The complex-load may also be placed within an industrial microwave multimode-cavity that employs two cavity-magnetrons. Figure 6 shows a simple schematic of how the Panasonic NE-1853 industrial microwave oven two magnetrons waveguide positioned top and bottom of the multimode-cavity and hence the dual microwave illumination[33]. As there is no rotating glass carousel, by default, the complex-load is placed central on the floor of the multimode-cavity where the bottom cavity-magnetron iris is located. In this case, the emerging scattered (incoherent) microwave energy (due to the rotating antenna) heats the 2.1 cm thick liquid-phase water directly before passing through the respirator then into cavity and finally undoing multiple reflections at the cavity wall. In contrast, the top cavity-magnetron illuminates the respirator first before passing into the liquid-phase water portion of the complex-load. In addition to direct line-of-sight-illumination, scattered microwave energy is reflected off the cavity walls back to the complex-load. Some of the scattered microwave energy may also enter back through the two waveguide irises and temporally disrupts the standing wave ratio (SWR) at the cavity-magnetron probe antenna, see equation (8) and (9). Figure 5 shows the waveguide SWR position in relation to the waveguide iris, multimode-cavity, and complex-load.

$SWR = \frac{1+|\Gamma|}{1-|\Gamma|}$ (8)

Where the 1+ corresponds to the addition of the incident and reflected E-Fields in the waveguide and the 1- corresponds to the subtraction of the incident and reflected E-filed in the waveguide. The modulus expression $|\Gamma|$ is the voltage refection coefficient, where V_r is the reflected voltage, and V_i is the incident voltage and P_r is the reflected power, and P_i is the incident power.

$\Gamma = \frac{V_r}{V_i} = \frac{\sqrt{p_r}}{\sqrt{p_i}}$ (9)

When the pulling frequency is within the operational bandwidth of cavity-magnetron, the microwave oven applies the full available power to the multimode-cavity. However, if outside the cavity-magnetron bandwidth power is lost, and in the extreme case stops working.

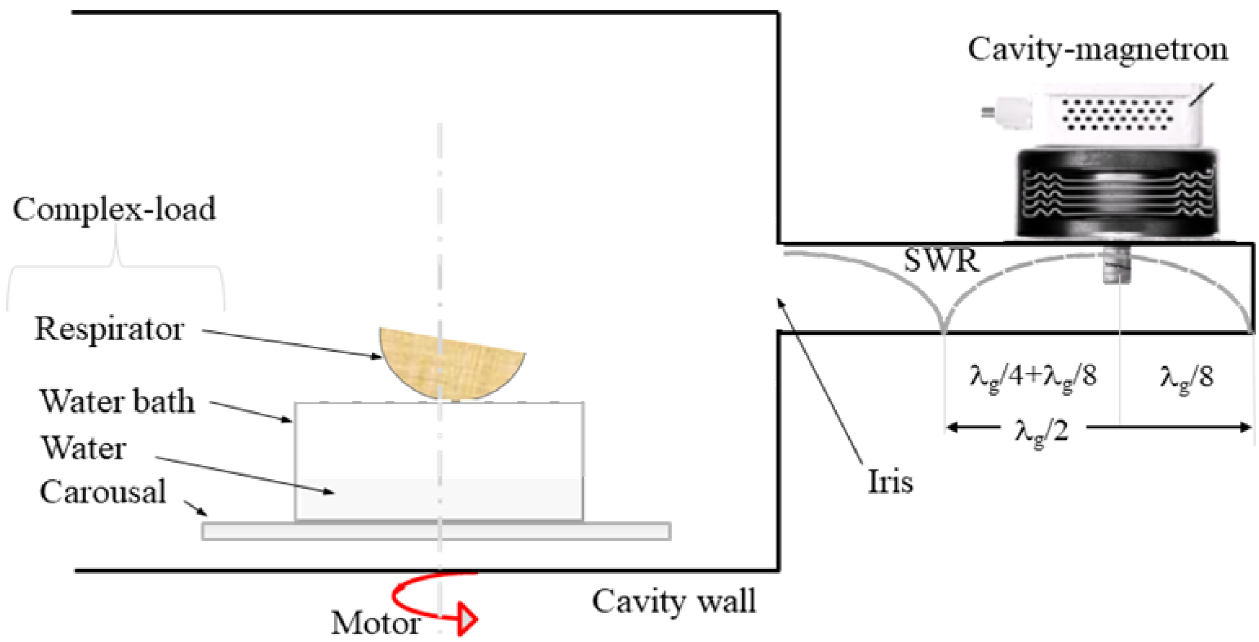

Fig-5: Cross-sectional schematic of a domestic microwave oven: cavity-magnetron, waveguide, SWR, iris, complex-load and carousel and motor. Left side of multimode-cavity removed for clarity.

Figure 5 depicts the typical case for a domestic microwave oven where the complex-load is placed on the central-axis of a glass carousel that is side-illuminated by a single cavity-magnetron. In this scenario, quasi-uniform dielectric volume heating of the complex-load is achieved as it rotates through the electromagnetic standing wave field patterns. The scattered microwave energy from the complex-load is reflected at the cavity walls, where some of the energy passes through the waveguide iris to alter the SWR at the cavity-magnetron probe.

The differing modes of batch volume dielectric heating may be sufficient for food-stuff where both conduction of heat energy through food tissue and convection of heated water though the liquid-phase are allowed take placed over a period of time once the microwave energy is turned-off . Now consider real-time batch MGS decontamination processing within a domestic microwave oven, where side-illumination of the open water bath complex-load occurs. In this case, load geometry and location to have role in the distribution of heat as the complex-load rotates. For example, a sphere containing water has a higher surface-to-volume ratio compared to cube or rectangular shape of similar volume, the sphere would be expected to heat more uniformly. However Lee et al[63] and references within, indicate that a spherical vessel with a narrow neck containing 200 ml of water placed in a fixed central position (therefore not stirred) will have a stratified heating profile with a superheated temperature layer forming at the free-surface and cooler layers towards the bottom in the initial stage of heating. It is only after a period of time that stratification is destroyed by convection mixing occurs. Given that an open water bath requires a free-surface area of approximately twice the area of that presented by respirator, cube and rectangular vessels, rotation of these vessels induce a heating modulation as the corners orientate two the side-illumination. This is because the microwave energy has to travel further within the water volume, along with synchronizing reflections as each consecutive corner passes through the side-illumination. The energy with the modulated reflections also have the potential of passing through waveguide iris, as incoherent energy, and alter the SWR at the cavity-magnetron probe antenna leading to frequency pulling of the cavity-magnetron pushing its power supply. This suggests that a low profile cylindrical open water bath (where *dp* approximates to the cylinder radius is constant for a given temperature) is a good compromise.

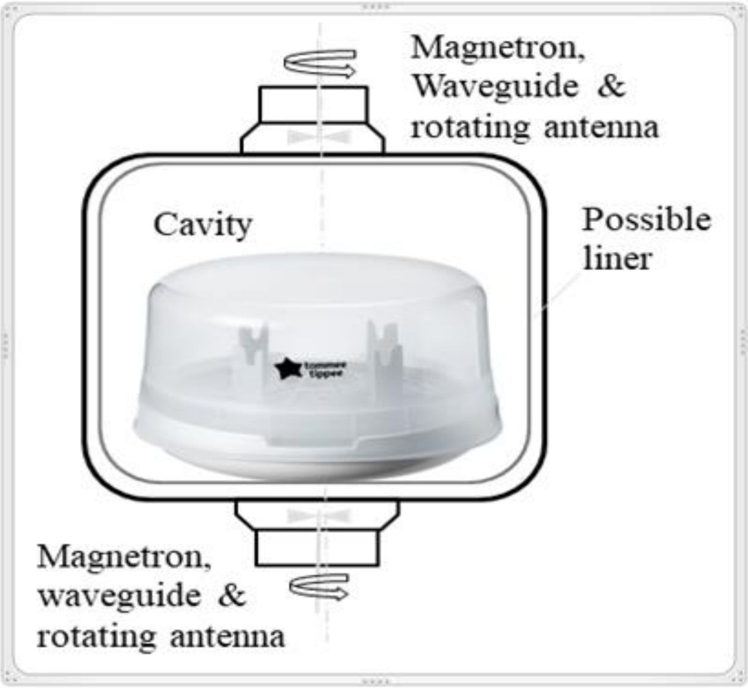

Fig-6: Front view schematic of an industrial microwave oven with sterilizer. The door and outer oven casing has been removed to show the complex-load intended position.

For the two cavity-magnetron industrial microwave oven, that microwave energy illuminates a non-rotating complex-load form both the bottom and top, and where the bottom microwave energy illuminates the open water bath, or sterilizer, water slab depth that approximates to one *dp*. This type of complex-load location further suggests uniform heating leads to faster steam generation for a single cavity-magnetron. This aspect of the MGS decontamination process requires further investigation, and in decoupling the top cavity-magnetron to investigate the top illumination effects.

3.6 Steam-respirator interactions within complex-load

It is generally postulated that in the first stage of dielectric volume heating the air relative humidity is increased, it then penetrates, and soaks the respirator body followed by the second stage of heating where the generated steam coalesces on to the respirator. In this process, the simultaneous action of microwave irradiation and heat transfer from steam to respirator are likely to be main the causes of virus inactivation. However, there is little information on how the water vapor and steam enters and pass through the multiple layers of the respirator. From a dielectric point of view, where 100^{o}C water has a *dp* of ~5.7 cm coalesced water within the millimeter thick respirator body will undergo dielectric volume heating (figure 2e). This aspect of the MGS process required further investigation.

3.7 Virus interaction with microwave irradiation

In 2014 Wu and Yao reported the rupture of the MS2 phage surface and damage to its RNA gene coding by direct microwave irradiation[39]. Before and after[39] of the MGS decontamination respirator papers used MS2 phage as a human surrogate for H1N1 and SARS-CoV-2. The microwave component associated with the inactivation MS2 points to a complex permittivity role in the activation process. Furthermore since the SARS-CoV-2 pandemic, interest has increased in microwave based (swept frequency 2 to 8 GHz and λ_o = 2.45 GHz) rapid diagnostic sensors for the detection of COVID-19. Both of which assume that the complex dielectric permittivity of the SARS-CoV-2 virus is similar to human blood (ε_r' ~57.5 to 42.5 and ε_r'' ~17 to 18; at 20 to 25). In the case of the swept frequency analysis the increase in frequency with SARS-CoV-2 indicates a reduction in reactance (capacitance, inductance, or a combination of both. This body of work[39,74] implies that the SARS-CoV-2 virus is likely to undergo dielectric heating as well as heat transfer from steam in the MGS decontamination process. To confirm this possibility further investigation is required.

4. Comments on cavity-magnetron rated and available power and temperature measurement

In batch MGS decontamination of respirators, the cavity-magnetron is invariably used in the continuous wave (CW) mode of operation. The rated CW power of cavity-magnetron is usually located at the back of the oven and within the manufactures accompanying documentation. The CW values relates to the maximum output power of the cavity-magnetron when impedance matched into a dumpy load, typically water, but not the power delivered in the multimode-cavity.

To make a meaningful power calculation of the cavity-magnetron, the available power within the multimode-cavity is required. This is performed using a standard calorimetry measurement[7,9,2 -31,41,63,67]. In addition, power density (W ft^3, or W L^{-1}) may be used to compare processes between different ovens. As the measure is a mathematical construct, care should be taken when rated and available cavity-magnetron powers are used.

The process energy budget relates to the rated, or available, power of the cavity-magnetron times the irradiated time: measured in the unit of Joule (J)[40, 41]. Given that the irradiated time varies between 60 to 180 seconds for most MGS decontamination processes, the cavity-magnetron warm-up time (3 s to 5 s [67]) does not significantly impact on the calculated total energy budget. For example, table 1 reveals that the Bergman et al[7] steam production has the potential to generate 41.7 L of steam, which is typically less than a half of Heimbuch et al[8] data (87.2 L of steam) and Lore et al[10] (98.8 L of steam). However, Zulauf et al[32] has the greatest potential of producing steam (136.6 L). The most plausible explanation for this outcome is that is the available power in Bergman's experiment has been measured and known to be an average of 750 W. Whereas; Heimbuch, Lore and Zulauf use rated cavity-magnetron powers values of 1000 to 1250 W within their oven cavities.

Monitoring the temperature of a material within an operational microwave oven is difficult as the use of earthed thermocouple probes generate sparks and arc that cause errors in the measurement instrumentation, microwave radiation into the environment[53]. To avoid these issues, liquid crystal irreversible temperature indicator strips can be used to provide temperature measurements on the respirator[33] as well as on ceramics[29,76] whilst temperature measurement of local liquid-phase water may be performed using a fiber optic thermometer probe[63].

5. SUMMARY

This paper reports upon the analysis of the dielectric properties of distilled-water, tap-water, N95-like respirator polymer material (f-PP), and where present the respirator metal (aluminum) nose clip, all of which are used in the MGS decontamination of N95-like respirator process. The analysis is performed at a microwave oven cavity-magnetron operational frequency of f_o ~2.24 GHz (l_o ~12.2 cm) within the environmental temperature of 20 to 25^{o}C, f-PP thermal deformation temperature region.

Firstly, it is proposed that N59-like respirator metal nose clip can be modeled as a quasi-transverse electromagnetic (TEM) microstrip, where at environmental temperatures the effective dielectric constant is defined by the surrounding polypropylene - air media. As the temperature increases to decontamination temperatures (70 to 100^{o}C), air is replaced with water vapor then stream causing the effective dielectric constant to increase and the phase velocity to decrease. Under these dynamic conditions, the imposed microwave wavelength is reduced producing open- and short-circuit nodes to bunch and move tangentially along the aluminum conductor causing high voltage stress regions at the open-circuits nodes to momentarily align with sharp edges and protrusions resulting (with sufficient energy) to produce sparks and arcs.

Secondly, a literature search revealed how the complex-load water volume, geometry, carousel multi-material, non-rotation and rotation orientation within the horizontal-plane alter heating uniformity and the possibility of frequency pulling of the cavity-magnetron and pushing of the cavity-magnetron power supply.

Finally, the links between complex-load dielectric parameters and cavity-magnetron stability complement the thermodynamics analysis of the batch MGS decontamination of N95-like respirator processing. The use of this knowledge allows process scale-out using process intensification principles, where the aim is to standardize decontamination outcome along with reducing energy budget.

Conflict of interest

The authors declare they have no conflicts of interest.

REFERENCES

1. A. Mardimae, M. Slessarev, J. Han, H. Sasano, N. Sasano. et al. Modified N95 mask delivers high inspired oxygen concentrations while effectively filtering aerosolized microparticles. Annals of Emergency Medicine. 48(4), 391-399, 2006
2. M.M. Weiss, D.E. Weiss, J.B. Weiss. Disrupting the transmission of influenza a: face masks and ultraviolet light as

control measures. American Journal Public Health. 97(S1), S32-37, 2007
3. https://assets.publishing.service.gov.uk/government/uploads/system/uploads/attachment_data/file/927770/exercise-cygnus-report.pdf
4. A.L.P. Silva, J.C. Prata, T.R. Walker, A.C. Duarte, W. Ouyang, D. Barcelò and T. Rocha-Santos. Increased plastic pollution due to COVID-19 pandemic: Challenges and recommendations. Chemical Engineering Journal. 405: 126683, 2021
5. N.B. Rodríguez, G. Formentini, C. Favi and M. Marconi. Engineering design process of face masks based on circularity and life cycle assessment in constraint of the covid-19 pandemic. Sustainability. 13, 4948, 2021
6. I. Oncioiu, I. Duca, M.A. Postole, G.C.G (Cretan), R. Gherghina and R-A. Grecu. Transforming the COVID-19 threat into an opportunity: the pandemic as a stage to the sustainable economy. Sustainability. 13, 2088, 2021
7. M.S. Bergman, D.J. Viscusi, B.K. Heimbuch, J D. Wander, A.R. Sambol, and R.E. Shaffer. Evaluation of multiple (3-cycle) decontamination processing for filtering facepiece respirators. Journal of Engineered Fibers and Fabrics. 5(4), 33-41, 2010.
8. B.K. Heimbuch, W.H. Wallace, K.R. Kinney, A.E. Lumley, C.Yu Wu, M-H Wo and J.D. Wander. A pandemic influenza preparedness study: use of energetic methods to decontaminate filtering facepiece respirators contaminated with H1N1 aerosols and droplets. American Journal of Infection Control. 39(1), pp. e1–e9, 2011.
9. E.M. Fisher, J.L. Williams, R. Shaffer. Evaluation of microwave steam bags for the decontamination of filtering facepiece respirators. PioS one. 6(4), 18585, 2011
10. M.B. Lore, B.K. Heimbuch, T.L. Brown, J.D. Wander and S.H. Hinrichs. Effectiveness of three decontamination treatments against influenza virus applied to filtering facepiece respirators. Annals of Occupational Hygiene. 56(1), 92-101, 2012
11. E.M. Fisher, J. Williams, and R.E. Shaffer. The effect of soil accumulation on multiple decontamination processing of N95 filtering facepiece respirator coupons using physical methods. Journal of the International Society for Respiratory Protection. 27(1), 16-16, 2010
12. D.J. Viscusi, M.S. Bergman, D.A. Novak, K.A. Faulkner, A. Palmiero, J. Powell and R.E. Shaffer. Impact of three biological decontamination methods on filtering facepiece respirator fit, odor, comfort, and donning ease. Journal of Occupational and Environmental Hygiene. 8: 426-436, 2011
13. T.F. Yap, Z. Liu, R. A. Shveda, and D.J. Preston. A predictive model of the temperature-dependent inactivation of coronaviruses. Applied Physics Letters. 117, 060601, 2020.
14. J.P. Abraham, B.D. Plourde and L. Cheng. Using heat to kill SAR-CoV-2. Rev. Med. Virol. 1-3, 2020
15. A.W.H. Chin, J.T.S. Chu, M.R.A. Perera, K.P.Y. Hui, H-L.Y, M.C.W. Chan, M. Peiris and L.L.M. Poon. Stability of SARS-CoV-2 in different environmental conditions. The Lancet Microbe. 1(1), e10, 2020
16. D.J. Viscusi, W.P. King, and R.E. Shaffer. Effect of decontamination on the filtration efficiency of two filtering facepiece respirator models. Journal of the International Society for Respiratory Protection. 24, 93-107, 2007
17. R.J. Fischer, D.H. Morris, N. van Doremalen, S. Sarchette, M.J. Matson, T. Bushmaker, C.K. Yinda, S.N. Seifert, A. Gamble, B.N. Williamson, S.D. Judson, E. de Wit, J.O. Lloyd-Smith and V.J. Munster. Effectiveness of N95 respirator decontamination and reuse against SARS-CoV-2 Virus. Emerging Infectious Diseases. 26(9), 2253-2255, 2020
18. M.A. Khan, A. Ikram, S. Savul , F.K. Lalani, M.A. Khan and M. Sarfraz. Decontamination and reuse of N95 Masks: a narrative review. Canadian Journal of Infectious Diseases and Medical Microbiology. 2020, 9 pages, 2020
19. A. Polkinghorne, J. Branley. Evidence for decontamination of single-use filtering facepiece respirators. Journal of Hospital Infection 105, 663-669, 2020
20. S. Gertsman, A. Agarwal, K. O'Hearn, R. Webster, A. Tsampalieros, N. Barrowman, M. Sampson, L. Sikora, E. Staykov, R. Ng, J. Gibson, T. Dinh, K. Agyei, G. Chamberlain and J.D. McNally. Microwave- and heat-based decontamination of N95 filtering facepiece respirators: a systematic review. Journal of Hospital Infection. 106, 536-530, 2020
21. N. Jacobs, K. Chan, V. Leso, A. D'Anna, D. Hollins and I. Iavicoli. A critical review of method fo decontaminating filtering facepiece respirators. Toxicology and Industrial Health. 36(9) 654-680, 2020
22. D. Paul, A. Gupta and A.K. Maurya. Exploring options for reprocessing of N95 filtering facepiece respirators (N95-FFRs) amidst COVID-19 pandemic: a systematic review. PLoS ONE 15(11), e0242474, 2020
23. K. Wharton and M. Rieker. N95 respirator decontamination and reuse: current state of the evidence. AANA Journal. 31-36, 2020
24. 3M Science. Applied to Life.™ Technical Bulletin March 20, 2020. Disinfection of filtering facepiece respirators.
25. L.F. Probst, A.T.G. Guerrero, A.I.de.Q. Cardoso, A.J. Grande, M.G. Croda, J. Venturini, M.C.de.C. Fonseca, A.M.M. Paniago, J.O. M. Barreto and S.M.do.V.L.de. Oliveira. Mask decontamination methods (model N95) for respiratory protection: a rapid review. Systematic Reviews. 10:219, 2021.
26. M.A. Schumm, J.E. Hadaya, N. Mody, B.A. Myers and M. Maggard-Gibbons. Filtering facepiece respirator (N95 Respirator) reprocessing a systematic review. JAMA. 325(13), 1296-1317, 2021
27. K. Seresirikachorn, V. Phoophiboon, T. Chobarporn, K. Tiankanon, S. Aeumjaturapat, S. Chusakul and K. Snidvongs. Decontamination and reuse of surgical masks and N95 filtering facepiece respirators during the

COVID-19 pandemic: A systematic review. Infection Control & Hospital Epidemiology. 42, 25-30, 2021
28. J.V. Loon, L. Veelaert, S.V. Goethem, R. Watts, S. Verwulgen, J.C. Verlinden and E.D.R Bois. Reuse of filtering facepiece respirators in the COVID-19 era. Sustainability. 13(2), 797, 2021
29. V.J. Law and D.P. Dowling. Converting a microwave oven into a plasma reactor: a review. International Journal of Chemical Engineering. 2018, (p12), 2018
30. V.J. Law and D.P. Dowling. Domestic microwave oven and fixed geometry waveguide applicator processing of organic compounds and biomaterials: a review. Global Journal of Researches in Engineering: A Mechanical and Mechanics Engineering. 18(2), 2018
31. V.J. Law and D.P. Dowling. The domestic microwave oven as a rapid prototyping tool. Analytical Chemical India Journal. 8(2), 2018.
32. K.E. Zulauf, A.B. Green, A.N. Nguyen Ba, T. Jagdish, D. Reif, R. Seeley, A. Dale, and J.E. Kirby. Microwave-generated steam decontamination of N95 respirators utilizing universally accessible materials. American Society Micoboilogy.11(3), e00997, 2020
33. M.J. Pascoe, A. Robertson, A. Crayford, E. Durand, J. Steer, A. Castelli, R. Wesgate, S.L. Evans, A. Porch and J-Y. Maillard. Dry heat and microwave-generated steam protocols for the rapid decontamination of respiratory personal protective equipment in response to COVID-19-related shortages. Journal of Hospital Infection. 106, 10-19, 2020.
34. R.N. Gedye, F. Smith and K.C. Westaway. The rapid synthesis of organic compounds in microwave ovens. Canadian Journal Chemistry. 66(1), 17-26, 1988
35. R.N. Gedye, W. Rank and K.C. Westaway. The rapid synthesis of organic compounds in microwave ovens. II. Canadian Journal Chemistry. 69(4), 706-711, 1991
36. Y. Tanaka, S. Fujiwara, D. Kataoka, T. Takagaki, S.Takano, S. Honda, M. Katayose, Y. Kinosita and Y. Toyoshima. Warming and sterilizing towels by microwave irradiation. Yonago Acta medica. 41, 83-88, 1998
37. D.K. Park, G. Bitton and R. Melker. Microbial inactivation by microwave radiation in the home environment. Journal of Environmental Health , 69(5), 17-24, 2006
38. M.J. Renfrew, M. McLoughlin and A. McFadden. Cleaning and sterilisation of infant feeding equipment: systematic review. Public Health Nutrition. 11(11), 1188-1199, 2008
39. Y.Wu and M. Yao. In situ airborne virus inactivation by microwave irradiation. Chinese Science Bulletin. 59(13), 1438-1445, 2014
40. V.J. Law and D.P. Dowling. The application of microwave generated steam ovens for the decontamination of respirators and face masks. Chemistry World Conference: webinar. September 1st 2021. https://chemistryworldconference.com/uploads/pdfs/final-program.pdf (acessed November 2021)
41. V.J. Law and D.P. Dowling. MGS decontamination of respirators: A thermodynamic analysis. GJRECS 1(1), 1-17, 2021
42. Z. Chen, G. Garcia-Jr, V. Arumugaswami and R.E. Wirz. Cold atmospheric plasma for SARS-CoV-2 inactivation. Physics of Fluids. 32, 111702, 2020
43. F. Capelli, S. Tappi, T. Gritti, A.C. de.A.S. Pinheiro, R. Laurita, U. Tylewicz, F. Spataro, G. Braschi, R. Lanciotti, F.G Galindo, V. Siracusa, S. Romani, M. Gherardi, V. Colombo, V. Sambri and P. Rocculi. Decontamination of food packages from SARS-CoV-2 RNA with a cold plasma-assisted system. Applied Science. 11, 4177, 2021
44. Z. Lei, J. Yang, Z. Zhuang and R. Roberge. Simulation and evaluation of respirator faceseal leaks using computational fluid dynamics and infrared imaging. Annals of Occupational Hygiene. 57(4), 493-506, 2012
45. D.F. Thambiraj, T. Chounthirath and G.A. Smith. Microwave oven-related injuries treated in hospital EDs in the United States, 1990 to 2010. American Journal Emergency Medicine. 31(6), 958-63, 2013
46. S. Bagirathan, K. Rao, S. Al-Benna and C.P. O'Boyle. Facial burns from exploding microwaved foods: case series and review. Burns. 42(2), e9-e12, 2016
47. R.K. Campos, J. Jin, G.H. Rafael, M. Zhao, L. Liao, G. Simmons, S. Chu, S.C. Weaver, W. Chiu, and Y. Cui. Decontamination of sars-cov-2 and other rna viruses from N95 level meltblown polypropylene fabric using heat under different humidities. ACS Nano. 14, 14017-14025, 2020
48. A. Mardimae, M. Slessarev J. Han, H. Sasano, N. Sasano, T. Azami, L. Fedorko, T. Savage, R. Fowler and J.A. Fisher. Modified N95 mask delivers high inspired oxygen concentrations while effectively filtering aerosolized microparticles. Annals of Emergency Medicine.48(4), 391-399, 2006
49. L. Liao, W. Xiao, M. Zhao, X. Yu, H, Wang, Q. Wang, S. Chu, Y. Cui. Can N95 respirators be reused after disinfection? And for how many times? ACS Nano , 1(5), 6348-6356, 2020
50. A. Ghosal, S. Sinha-Ray, A.L. Yarin and B. Pourdeyhimi. Numerical prediction of the effect of uptake velocity on three-dimensional structure, porosity and permeability of meltblown nonwoven laydown. Polymer. 85, 19–27, 2016
51. H. Zhang, N. Liu, Q. Zeng, J. Liu, X. Zhang, M. Ge, W. Zhang, S. Li, Y. Fu and Y. Zhang. Design of polypropylene electret melt blown nonwovens with superior filtration efficiency stability through thermally stimulated charging. Polymer. 12, 2341, 2020
52. M. Bhattacharya, T. Basak. A review on the susceptor assisted microwave processing of materials. Energy. 97, 306-338, 2006

53. S. Dąbrowska, T. Chudoba, J. Wojnarowicz and W. Łojkowski. Current trends in the development of microwave reactors for the synthesis of nanomaterials in laboratories and industries: a review. Crystals. 8, 379, 2018
54. A.H. Abdelgwad, T.M. Said. Measured dielectric permittivity of chlorinated drinking water in the microwave frequency range. IEEE 15th Mediterranean Microwave Symposium (MMS). pp. 1-4, 2015
55. V.V. Komarov and J. Tang. Dielectric permittivity and loss factor for tap water at 915 mhz. Microwave and Optical Technology Letters. 42(5), 419-420, 2004
56. A.J. Burr. Dielectric properties of polymer at microwave frequencies. Polymer. 26(7), 962-977,1985
57. B. Riddle and J. Baker-Jarvis. Complex permittivity measurements of common plastics over variable temperatures. IEEE Transactions on microwave Theory and Techniques. 51(3), 727-733, 2003
58. S.Z.A. Dabbak, H.A. Illias, B.C. Ang, N.A.A. Latiff and M.Z.H Makmud. Electrical properties of polyethylene/polypropylene compounds for high-voltage insulation. Energies. 11(6), 1448, 2018
59. T.C.M. Chung. Functionalization of polypropylene with high dielectric properties: applications in electric energy storage. Green and Sustainable Chemistry. 2, 29-37, 2012
60. I. Armentano, M. Barbanera, E. Carota, S. Crognale, M. Marconi, S. Rossi, G. Rubino, M. Scungio, J. Taborri, and G. Calabrò. Polymer materials for respiratory protection: processing, end use, and testing methods. Appl. Polym. Mater. 3, 531-548, 2001
61. J. Fayos-Fernández, I.P. Conesa, J. Monzó-Cabrera, S.del.P. León and J.C.A. González. Temperature-dependent complex permittivity of several electromagnetic susceptors at 2.45 GHz. Ampere Newletter. 55, 2-8, 2018.
62. V.J. Law. Microwave near-field plasma probe. Vacuum. 51(3), 463-468, 1998
63. G.L. Lee, M.C. Law and V.C.C. Lee. Numerical modelling of liquid heating and boiling phenomena under microwave irradiation using OpenFOAM. International journal of heat and mass transfer. 148, 119096, 2020
64. S.P. Yeong, M.C. Law, V.C.C. Lee and Y.S. Chan. Modelling batch microwave heating of water. IOP Conference Series: Materials Science and Engineering. 217(1), 012035, 2017
65. M.D. Anguelova. Complex dielectric constant of sea foam at microwave frequencies. J Geophysical Research. 113, C08001, 2008
66. H. Looyenga. Dielectric constants of heterogeneous mixtures. Physica. 31(3), 401-406 , 1965
67. S.S.R. Geedipalli, V. Rakesh and A.K. Datta Modeling the heating uniformity contributed by a rotating turntable in microwave ovens. Journal of Food Engineering. 82(3), 359-368, 2007
68. J. Ye, T. Hong, Y. Wu , L. Wu, Y. Liao, H. Zhu, Y. Yang and K. Huang. Model stirrer based on a multi-material turntable for microwave processing materials. Materials. 10(2), 95, 2017
69. J. Houšová and K. Hoke. Microwave heating - the influence of oven and load parameters on the power absorbed in the heated load. Czech J. Food Sci. 20(3), 117-124, 2002
70. F.E. Ross and W.H. Hunter. Rotating antenna for microwave oven. US Patent. 4,641,006 (issued Feb 3, 1987)
71. Operating instructions for commercial use. Models No. NE-1843/NE-1853 microwave ovens. Panasonic Corporation. https://www.regale.co.uk/wp-content/uploads/2014/04/1843_1853-Operators-Manual.pdf (accessed November 2021)
72. V.J. Law, D.P. Dowling. Microwave oven plasma reactor moding and its detection. 12th Chaotic Modeling and Simulation International Conference. Springer Proceedings in Complexity. Springer, Cham. Chap 14,157-179, 2019
73. J. Ahmed and H.S. Ramasamy. Microwave Pasteurization and Sterilization of Foods. Handbook of Food Preservation, Second Edition. ed S. Rahman. CRC Press. Chap 28, 709-730, 2007
74. Y.I. Abdulkarim, H.N. Awl, F.F. Muhammadsharif, K.R. Sidiq, S.R. Saeed, M. Karaaslan, S. Huang, H. Luo, L. Deng. Design and study of a coronavirus-shaped metamaterial sensor stimulated by electromagnetic waves for rapid diagnosis of covid-19. arXiv preprint arXiv:2009.08862, 2020
75. D.M. Elsheakh, M.I. Ahmed, G.M. Elashry, S.M. Moghannem, H.A. Elsadek, W.N. Elmazny, N.H. Alieldin and E.A. Abdallah. Rapid detection of coronavirus (covid-19) using microwave immunosensor cavity resonator. Sensors. 21, 702, 2021
76. V.J. Law, A.J. Kenyon., DC. Clary and I. Batty. A noninvasive rf probe for the study of ionization and dissociation processes in technological plasmas. Journal of Applied Physics. 86(8), 4100-4106, 1999
77. V.J. Law and D. Tait, Microwave plasma cleaning of ion implant ceramic insulators. Vacuum. 49(4,), 273-278, 1998
78. B.H. Erné and P. Snetsinger. Thermodynamics of water superheated in the microwave oven. Journal of Chemical Education. 77(10), 1309-1310, 2000
79. D.J. Visccus, M.S. Bergman, B.C. Eimer and R.E. Shafaffer. Evaluation of five decontamination methods for filtering facepiece respirators. Ann. Occup. Hyg. 53(8), 815–827, 2009
80. Industrial microwave heating installations. Test methods for the determination of power output. BS EN 61307, 2011